Breast Cancer Assessment With Pulse-Echo Speed of Sound Ultrasound From Intrinsic Tissue Reflections: Proof-of-Concept

Ruby, Lisa ; Sanabria, Sergio J ; Martini, Katharina ; Dedes, Konstantin J ; Vorburger, Denise ; Oezkan, Ece ; Frauenfelder, Thomas ; Goksel, Orcun ; Rominger, Marga B

Abstract: PURPOSE The aim of this study was to differentiate malignant and benign solid breast lesions with a novel ultrasound (US) technique, which measures speed of sound (SoS) using standard US transducers and intrinsic tissue reflections and scattering (speckles) as internal reference. MATERIALS AND METHODS This prospective, institutional review board-approved, Health Insurance Portability and Accountability Act-compliant prospective comparison study was performed with prior written informed consent from 20 women. Ten women with histological proven breast cancer and 10 with fibroadenoma were measured. A conventional US system with a linear probe was used for SoS-US (SonixTouch; Ultrasonix, Richmond, British Columbia, Canada). Tissue speckle reflections served as a timing reference for the US signals transmitted through the breasts. Relative phase inconsistencies were detected using plane wave measurements from different angular directions, and SoS images with 0.5-mm resolution were generated using a spatial domain reconstruction algorithm. The SoS of tumors were compared with the breast density of a larger cohort of 106 healthy women. RESULTS Breast lesions show focal increments ΔSoS (meters per second) with respect to the tissue background. Peak ΔSoS values were evaluated. Breast carcinoma showed significantly higher ΔSoS than fibroadenomas ([INCREMENT]SoS $>$ 41.64 m/s: sensitivity, 90%; specificity, 80%; area under curve, 0.910) and healthy breast tissue of different densities (area under curve, 0.938; sensitivity, 90%; specificity, 96.5%). The lesion localization in SoS-US images was consistent with B-mode imaging and repeated SoS-US measurements were reproducible. CONCLUSIONS Using SoS-US, based on conventional US and tissue speckles as timing reference, breast carcinoma showed significantly higher SoS values than fibroadenoma and healthy breast tissue of different densities. The SoS presents a promising technique for differentiating solid breast lesions.

DOI: https://doi.org/10.1097/RLI.0000000000000553

Breast Cancer Assessment With Pulse-Echo Speed of Sound Ultrasound From Intrinsic Tissue Reflections
Proof-of-Concept

Lisa Ruby, MD, Sergio J. Sanabria, PhD,*† Katharina Martini, MD,* Konstantin J. Dedes, MD,‡ Denise Vorburger, MD,‡ Ece Oezkan, PhD,† Thomas Frauenfelder, MD,* Orcun Goksel, PhD,† and Marga B. Rominger, MD**

Purpose: The aim of this study was to differentiate malignant and benign solid breast lesions with a novel ultrasound (US) technique, which measures speed of sound (SoS) using standard US transducers and intrinsic tissue reflections and scattering (speckles) as internal reference.

Materials and Methods: This prospective, institutional review board–approved, Health Insurance Portability and Accountability Act-compliant prospective comparison study was performed with prior written informed consent from 20 women. Ten women with histological proven breast cancer and 10 with fibroadenoma were measured. A conventional US system with a linear probe was used for SoS-US (SonixTouch; Ultrasonix, Richmond, British Columbia, Canada). Tissue speckle reflections served as a timing reference for the US signals transmitted through the breasts. Relative phase inconsistencies were detected using plane wave measurements from different angular directions, and SoS images with 0.5-mm resolution were generated using a spatial domain reconstruction algorithm. The SoS of tumors were compared with the breast density of a larger cohort of 106 healthy women.

Results: Breast lesions show focal increments ΔSoS (meters per second) with respect to the tissue background. Peak ΔSoS values were evaluated. Breast carcinoma showed significantly higher ΔSoS than fibroadenomas (ΔSoS > 41.64 m/s: sensitivity, 90%; specificity, 80%; area under curve, 0.910) and healthy breast tissue of different densities (area under curve, 0.938; sensitivity, 90%; specificity, 96.5%). The lesion localization in SoS-US images was consistent with B-mode imaging and repeated SoS-US measurements were reproducible.

Conclusions: Using SoS-US, based on conventional US and tissue speckles as timing reference, breast carcinoma showed significantly higher SoS values than fibroadenoma and healthy breast tissue of different densities. The SoS presents a promising technique for differentiating solid breast lesions.

Key Words: differentiation, detection, breast, density, cancer, fibroadenoma, speed of sound, tumor, breast lesion, ultrasound

(*Invest Radiol* 2019;00: 00–00)

With an estimate of approximately new 1.7 million cases per year worldwide, breast cancer is the most common malignant tumor and the leading cause of cancer-related death in women worldwide.[1] Fibroadenomas present the most common benign breast lesions.[2] Mammography is the current criterion standard for breast cancer screening. However, due to the inherent radiation exposure, reduced sensitivity in dense breasts as well as the patient discomfort caused by tissue compression additional methods are needed. Supplemental ultrasound (US) imaging has been shown to have the potential to detect small[3] and mammographically obscured[4,5] tumors and to distinguish fibroadenomas from triple-negative breast cancer.[6] Elastography (strain and shear wave) increased accuracy and specificity of US with respect to US alone (B-mode) or US with Doppler imaging in the distinction of small, oval, or round triple-negative breast cancer from fibroadenoma.[7] For breast cancers, shear wave elastography demonstrated a correlation with both histopathological and mechanical tumor properties.[8] However, a major limitation of both US[9] and elastography[10] is the dependency on the examiners' experience and few standardization. Currently, US differentiation of solid breast lesions is based on the qualitative analysis of tumor margins and geometry (for instance, spiculation, boundary uniformity, ovality) of the lesions, whereas the echogenicity of the lesion on its own does not provide enough contrast for differentiation. In the case of elastography, quantitative biomarkers (strain ratios, shear wave velocity) can be provided as surrogates to stiffness.[11,12] However, these measurements can be subject to confounders, such as dependency on tissue precompression and region of interest, and special care must be taken to avoid or interpret artifacts.[13] Moreover, in some cases, cancers do not appear as stiff lesions.[14]

Breast cancer imaging is currently a rapidly changing world with a constant flux of new ideas for diagnostics and treatment[15] methods. A variety of methods have been developed, which allow for objective tissue quantification for both MRI[16] and x-rays.[17,18] Ultrasound imaging is not foreign to this trend, with continuous advances based on elastography,[19,20] contrast agents,[21] optoacoustic imaging,[22,23] and texture analysis,[24] among others. In recent years, an alternative US technology, US computed tomography (USCT), has been developed for tissue quantification, and has shown potential to both detect and differentiate breast lesions.[25–27] Current USCT systems use a transmission US setup, in which the breasts are immersed in a water bath, and dedicated ring transducers are used to transmit and receive US pulses along multiple paths. Apart from conventional reflectivity images (B-mode), this allows imaging additional quantitative parameters of longitudinal US waves, such as the speed of sound (SoS) and the acoustic attenuation at multiple frequencies. These parameters have been shown to be independent from stiffness surrogates provided by elastography, and thus may contain additional information for tumorous tissue detection and differentiation.[25–29]

Ultrasound computed tomography methods are dedicated systems for breast imaging. It would, however, be desirable to add quantitative biomarkers also to standard US systems based on hand-held US array probes. The SoS imaging would then be an additional functionality of the US machine, which, similar to Doppler or elastography, would be overlaid to the B-mode images, and allow detection and quantification of breast lesions. Some works have attempted to obtain average SoS values in soft tissues from the deblurring of US images.[30–32] More recently, several research works have attempted to obtain spatially resolved SoS images based on US probes and analysis of reflected US

Received for publication November 26, 2018; and accepted for publication, after revision, January 13, 2019.

From the *Institute of Diagnostic and Interventional Radiology, University Hospital Zurich; †Computer-Assisted Applications in Medicine, ETH Zurich; and ‡Breast Cancer Center, Comprehensive Cancer Center Zurich, University Hospital of Zurich, Zurich, Switzerland.

Lisa Ruby and Sergio J. Sanabria both contributed equally to the manuscript.

Conflicts of interest and sources of funding: This project has been generously supported by a donation from Hans-Peter-Wild to the University Hospital Zurich Foundation. Sergio Sanabria was funded by the ETH Pioneer Fellowship.

All authors contributed substantially to the conception and design, acquisition of data, or analysis and interpretation of data, as well as drafting the article or revising it critically for important intellectual content.

Final approval of the version to be published.

Agreement to be accountable for all aspects of the work in ensuring that questions related to the accuracy or integrity of any part of the work are appropriately investigated and resolved.

Correspondence to: Marga B. Rominger, MD, Institute of Diagnostic and Interventional Radiology, University Hospital Zürich, Rämistrasse 100, 8091 Zürich. E-mail: Marga.Rominger@usz.ch.

ISSN: 0020-9996/19/0000–0000
DOI: 10.1097/RLI.0000000000000553

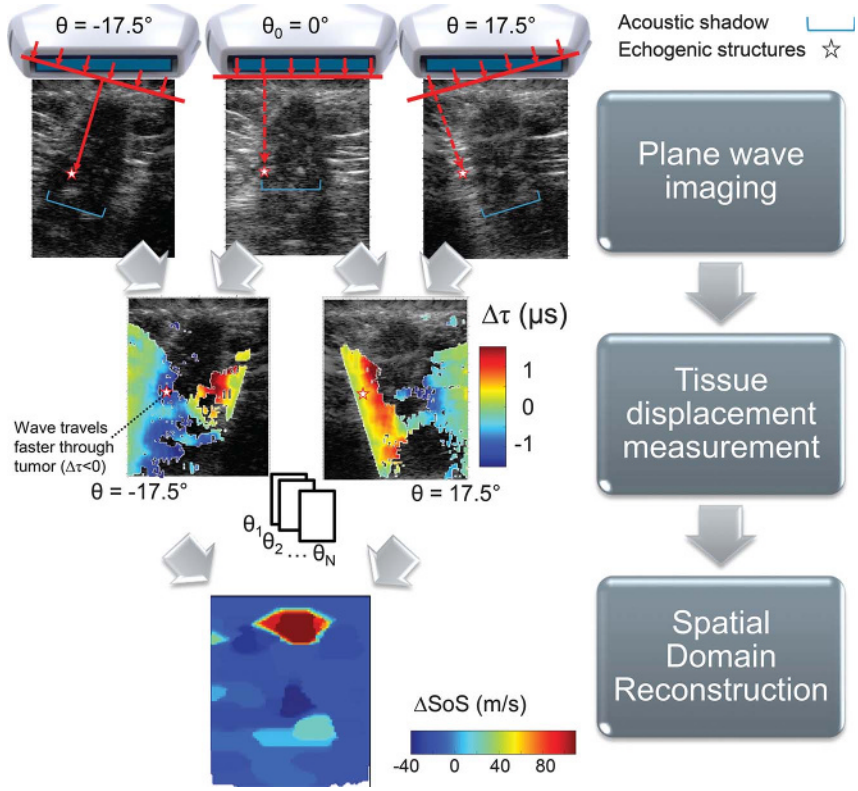

FIGURE 1. Speed of sound (SoS) image reconstruction steps[34] for an invasive ductal carcinoma (IDC) lesion with speckles-based SoS method. A, Ultrasound plane wave images of the lesion are generated from multiple directions θ. B, Apparent tissue displacements are measured with a speckle tracking algorithm, only measurements over a correlation threshold are preserved. C, A spatial domain reconstruction algorithm provides an SoS image. The lesion mask annotated from B-mode is used for quantitative evaluation of the SoS increment ▵SoS in the lesion (m/s).

signals.[32–34] Two-dimensional (2D) SoS-US is a novel technique, which uses a conventional US system to measure SoS in breast tissue (Fig. 1).[34] External reflectors in combination with hand-held US probes have been used to measure SoS (external reflector-based method).[35,36] Sanabria et al.[34] have shown the potential of tissue reflections and scattering (speckles) to serve as internal reflector and timing references, which leads to even easier measurement operability for SoS imaging by hand-held probes.

The goal of this study was to investigate the feasibility of SoS-US to differentiate breast cancer from fibroadenoma and healthy breast tissue using conventional US probes and the SoS imaging method using tissue reflections (speckles-based SoS method).

MATERIALS AND METHODS

Study Design

This prospective, single-institution study was approved by the institutional review board and local ethics committee. Informed written consent was obtained from all women. Twenty women presenting with sonographic solid breast lesions that required biopsy were examined at the University Hospital of Zurich between September 2016 and August 2017. B-mode and 2D SoS of each lesion were performed. The specimen of the biopsied lesion sample was sent to the Institute of Pathology for histopathological assessment. Inclusion criterion was a pathologic diagnosis of invasive lobular carcinoma (ILC), invasive carcinoma (IDC) or fibroadenoma. Twenty women agreed to participate in the study. No selection was made with regard to the patient's age or breast density. The median age was 42 years for the fibroadenoma patients (ranging from 17–79 years) and 79 years for the carcinoma patients (ranging from 57–89 years). The patient characteristics are listed in Tables 1 and 2.

The SoS of the tumors (n = 20) of this study were compared with the SoS of breast tissue segments (retromamillary, inner, and outer) of 106 healthy women.[35] Speckles-based 2D SoS-US images as well as mammographic breast density categories (A, almost entirely fatty; B, scattered areas of fibroglandular density; C, heterogeneously dense; and D, extremely dense) according to the American College of Radiology (ACR) Breast Imaging Reporting and Data System (BIRADS) fifth edition[37] were acquired in 318 tissue segments.

Speed of Sound Ultrasound

A commercially available US system (SonixTouch; Ultrasonix, Richmond, British Columbia, Canada) with a 9-MHz linear US array (L14/5–38) was used for US imaging. The US probe has 128 elements, with a pitch of 0.3 mm between elements, an element elevation of 7 mm and a total aperture of 38 mm. B-mode images were used for lesion navigation and acquired from the clinical interface of the device, which incorporates standard beam-forming and scan conversion filters. For SoS imaging, a multichannel data acquisition board (SonixDAQ, Ultrasonix) was used to simultaneously collect prebeamformed data from all probe elements with 40-MHz sampling rate and 12 bits per sample. Then, raw data, also called multistatic data or full-matrix data, were acquired by sequentially transmitting a pulse with an aperture of 1 element and recording the received echoes with all other elements. In total, 128 × 128 = 16′384 prebeamformed lines were recorded (about 100 MB/measurement). A custom add-on software and an interface developed for this purpose were used for data acquisition and SoS image evaluation.

Principle From SoS-US Image Reconstruction

The generation of SoS-US images out of tissue reflections has been described and validated with numerical simulations by Sanabria et al.[34]

TABLE 1. Clinical Characteristics of n = 20 Patients with Carcinoma Lesions

	CA1	CA2	CA3	CA4	CA5	CA6	CA7	CA8	CA9	CA10
Breast density	B	A	C	NA	B	B	A	A	C	B
Bra cup	A	B	B	B	B	NA	NA	NA	B	B
Age	80	66	69	88	68	89	79	79	82	57
Menopausal status	Post	Post	Post	Pre	Post	Post	Post	Post	Post	Post
BMI	NA	22.0	24.6	23.9	NA	NA	NA	NA	28.7	NA
Histology	IDC	IDC	IDC	IDC	IDC	IDC	IDC	IDC	ILC	ILC
Location lesion	LO	LM	RM	LO	LM	RO	LO	RO	LM	RO
Horizontal diameter, mm	7.2	9.2	6.1	11.2	27.3	15.7	11.1	12.9	18.9	8.8
Vertical diameter, mm	4.5	9.7	5.2	8.9	22.2	24.4	12.5	20.6	14.3	10.1
ΔSoS, m/s	47.7	59.7	42.7	14.2	93.1	106.7	113.6	79.2	118.0	73.3
ΔSoS classification	Malignant	Malignant	Malignant	Benign	Malignant	Malignant	Malignant	Malignant	Malignant	Malignant

NA indicates not available; BMI, body mass index; RI, right inner; RM, right retromamillary; RO, right outer; LI, left inner; LM, left retromamillary; LO, left outer; IDC, invasive ductal carcinoma; ILC, invasive lobular carcinoma.

The main steps are summarized in Figure 1. When US waves are incident on tissue microstructure, diffuse scattering occurs, which is responsible for the gray shade texture observed in US images (speckle). The reflecting targets (so-called scatterers) are smaller than the wavelength, leading to uniform scattering in all directions. Hence, the tissue texture in the images does not change significantly with the angle of incidence of the wave.[38,39] In breast tissue, scattering is mainly produced by fat and glandular cells, which show isoechoic appearance; thin, echogenic Cooper ligaments structures; and intensely echogenic stromal fibrous tissue.[40]

By coregistering US images acquired from different angular directions, apparent tissue displacements can be measured, which are caused by time shifts of the US wave travelling through regions with different SoS properties. A spatial domain reconstruction algorithm[34] is then used to reconstruct an SoS image from the tissue displacements. In analogy to compression sensing algorithms,[41] spatial domain reconstruction uses regularization to achieve reconstructions, which are robust to missing/noisy displacement data and enhance delineation of focal lesion geometries. The data acquisition and reconstruction settings are the same as in the experiments shown by Sanabria et al.[34] with the same regularization used for all clinical reconstructions. The SoS images are reconstructed with a pixel size of 0.5 mm in the same coordinate frame as the B-mode images. Displacement measures with low correlation coefficient ($r < 0.3$) are excluded. The algorithm evaluates absolute SoS variations from the average background breast SoS value, referred as ΔSoS, as a quantitative imaging biomarker. ΔSoS is expressed in meters per second (m/s).

The maximum value of the resulting SoS images is evaluated and used for classification between healthy tissue, fibroadenoma, and carcinoma tissue. For fibroadenoma and carcinoma differentiation, additionally, closed loop lesion masks were annotated in the B-mode images by an experienced sonographer, and the maximum SoS value was evaluated within these masks. Peritumoral tissue region was also considered by dilating the annotated masks by a defined radius and then reevaluating SoS values within the dilated masked regions.

SoS-US Breast Examination

Three experienced (25, 15, and 15 years of experience, respectively) breast sonographers performed the examinations. There were no differences between them in doing the examination. All 3 sonographers used a standardized protocol measuring SoS in the plane showing the greatest diameter of the tumor.

First, a conventional US examination (B-mode) is carried out in the clinical mode of the US machine, and the US probe is navigated to a

TABLE 2. Clinical Characteristics of n = 10 Patients with Fibroadenoma Lesions

	FA1	FA2	FA3	FA4	FA5	FA6	FA7	FA8	FA9	FA10
Breast density	NA	NA	NA	NA	NA	NA	C	A	C	B
Bra cup	A	B	B	B	B	NA	NA	NA	B	B
Age	17.0	22.0	30.0	25.0	46.0	38.0	55.0	79.0	78.0	51.0
Menopausal status	Pre	Pre	Pre	Pre	Pre	Pre	Post	Post	Post	Peri
BMI	21.8	20.8	25.2	19.4	23.0	NA	NA	NA	NA	28.4
Histology	FA	FA	FA	FA	FA	FA	FA	FA	FA	FA
Location lesion	LI	LI	LM	LM	LO	LM	LM	RM	LO	LO
Horizontal diameter, mm	9.0	8.0	25.4	5.1	4.1	18.1	10.5	22.8	8.6	4.7
Vertical diameter, mm	10.8	6.3	13.8	5.4	3.8	3.4	11.6	5.4	4.2	3.4
ΔSoS, m/s	7.7	7.4	15.7	79.1	13.7	7.6	41.6	4.9	43.2	13.8
ΔSoS classification	Benign	Benign	Benign	Malignant	Benign	Benign	Benign	Benign	Malignant	Benign

NA indicates not available; BMI, body mass index; RI, right inner; RM, right retromamillary; RO, right outer; LI, left inner; LM, left retromamillary; LO, left outer; FA, fibroadenoma; IDC, invasive ductal carcinoma; ILC, invasive lobular carcinoma.

2D plane containing the lesion of interest. The size of the lesion is assessed in 3 planes, and the plane with the largest lesion diameter is selected. Then US multistatic data are acquired at the lesion plane with the same US probe. The data acquisition is performed in less than 0.1 second (frame rate >10 Hz). The present US system has a hardware switching delay between clinical mode and multistatic data acquisition mode of approximately 30 seconds. During this time, the sonographer must hold the probe with respect to the patient to avoid losing the region of interest. The SoS images are then automatically generated and displayed as a color overlay to B-mode images, with an adjacent quantitative scale of ΔSoS (m/s) (Figs. 2, 3). The bottom and lateral edges of the ΔSoS images are subject to speckle decorrelation and beamforming artifacts and were excluded from the evaluation (radius, 8.4 mm). For differential diagnosis, we used both the maximum ΔSoS value within the reconstructed SoS image (Fig. 4) and the maximum ΔSoS value within a region of interest around the lesion as visible in the B-mode image (Figs. 5,6).

Statistical Analysis

Statistical analysis was performed using Matlab (2014a, The MathWorks Inc, Natick, MA). Analysis of variance (ANOVA) was used for comparison of healthy breast segments, carcinomas, and fibroadenomas. A P value less than 0.05 was considered to indicate statistical significance. Receiver operating characteristic (ROC) analysis was performed with MedCalc 18.2.1 (2018, Ostend, Belgium) to evaluate area under curve (AUC). For illustration, MedCalc also automatically calculates sensitivity and specificity based on the optimum cutoff point for the test sample size, which

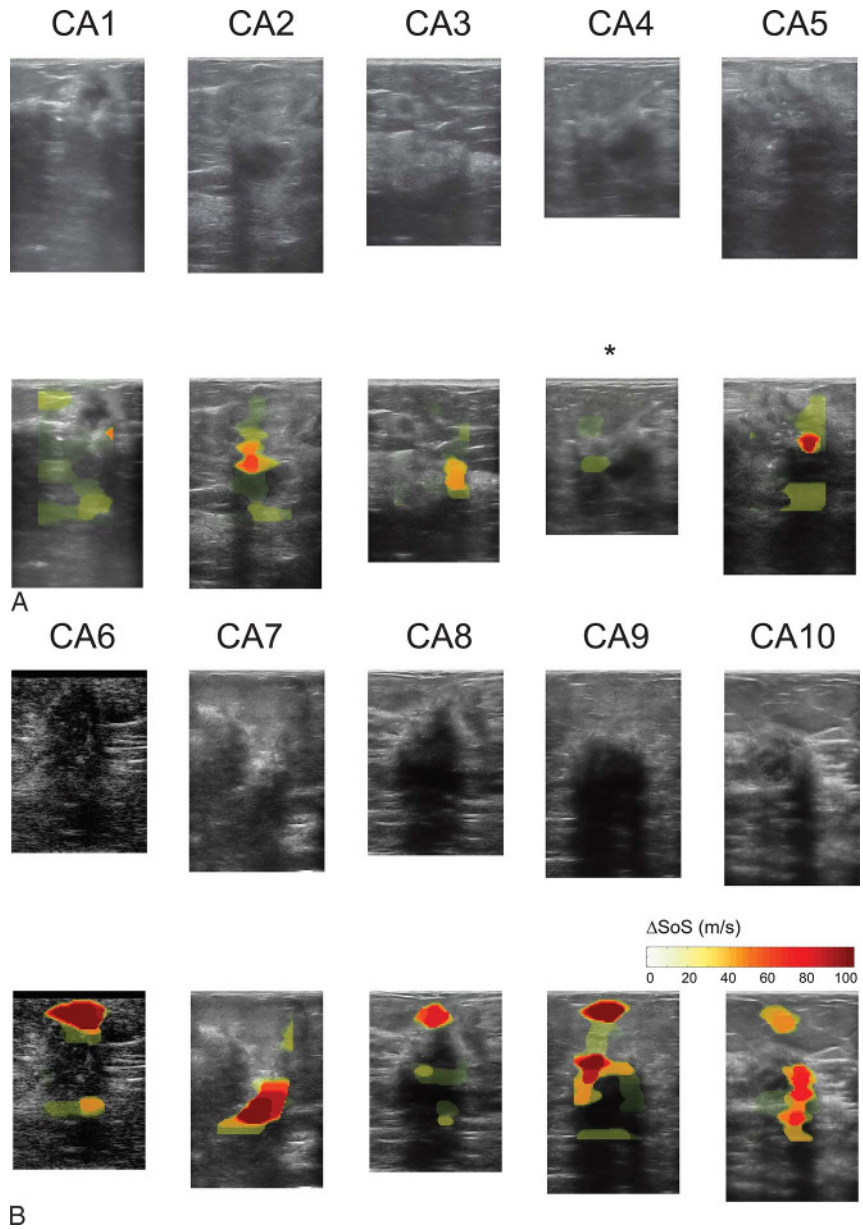

FIGURE 2. B-mode (first and third rows) and speed of sound images (second and fourth rows) for carcinoma lesions. There was one false-negative (CA4), which is marked with an asterisk, corresponding to an invasive carcinoma (IDC) with 11.2 mm diameter in the retromamiliary segment of a heterogeneously dense (ACR type C) breast.

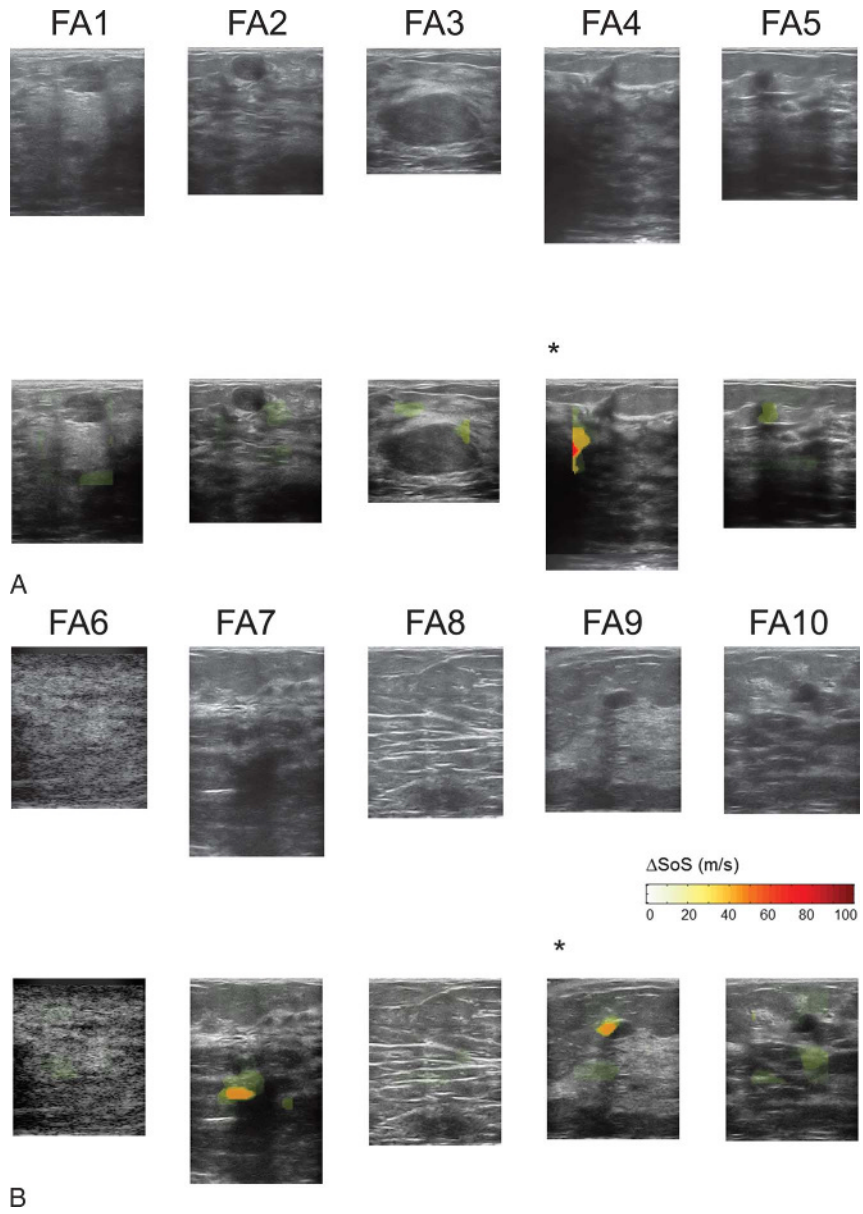

FIGURE 3. B-mode (first and third rows) and speed of sound images (second and fourth rows) for fibroadenoma lesions. There were 2 false-positives FA4 and FA9, which are marked with an asterisk. FA4 shows high ΔSoS values at the left image edge, where poor acoustic coupling is also observed. FA9 shows ΔSoS = 43.2 m/s, which is very close to the cutoff value.

is calculated with prevalence of 0.5 for both groups and same cost of false- and true-positive and negative decisions.[42]

RESULTS

Twenty (100%) of 20 measurements were successful. Fibroadenomas had diameters between 4.1 and 25.4 mm (median, 8.8 mm), whereas the carcinomas were between 6.1 and 27.3 mm (median, 11.2 mm). B-mode and SoS images, together with B-mode/SoS overlays are shown in Figure 2 for carcinoma and Figure 3 for fibroadenoma. Based on the evaluation of the full reconstructed SoS images, there was a significant difference between fibroadenoma and carcinoma ($P < 0.001$; Fig. 4A). After ROC analysis, the criterion ΔSoS greater than 41.64 m/s provided sensitivity of 90%, specificity of 80%, and AUC of 0.910 (Fig. 4B).

Nine of 10 carcinomas are characterized by higher SoS values, which show red spots in the images. There was 1 false-negative (CA4), corresponding to an IDC with 11.2 mm diameter in the retromamiliary segment of a heterogeneously dense (ACR type C) breast (Table 1). Eight of 10 fibroadenomas were correctly classified. There were 2 false-positives FA4 and FA9. FA4 shows high ΔSoS values at the left image edge, where poor acoustic coupling is also observed. FA9 shows ΔSoS = 43.2 m/s, which is very close to the cutoff value (Table 2). We did not observe significant differences between ΔSoS for carcinoma in breasts of different densities. Incidentally, the largest ΔSoS = 118.0 m/s was observed for patient CA9, which has a dense breast (ACR type C). The comparison of ΔSoS between IDC (n = 8) and ILC (n = 2) did not show a significant difference (*t* test $P = 0.367$).

Second, the SoS was evaluated based on the annotated lesion regions in the B-mode images. Seven of 10 lesions show a ΔSoS centroid within the B-mode lesion annotation region (yellow dotted line in

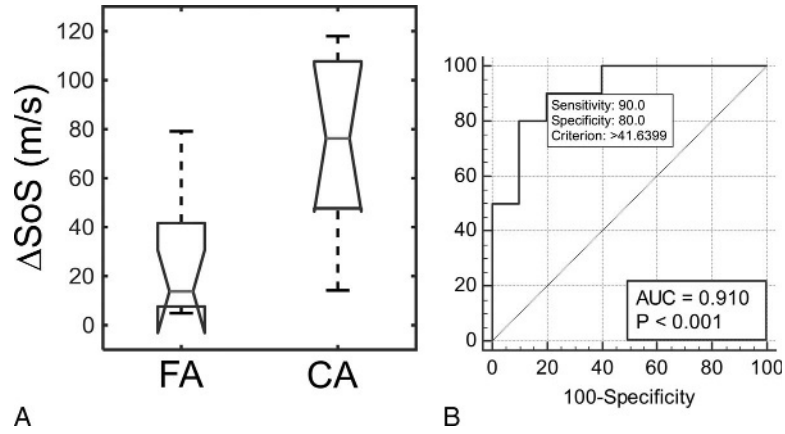

FIGURE 4. ANOVA (A) and ROC (B) plots for differentiation of fibroadenoma (FA) and carcinoma (CA). The evaluation is based on the fully reconstructed SoS image.

Fig. 6). CA1 has a centroid within the peritumorial region and CA3 outside the annotated lesion region. Inclusion of a peritumoral region of 6 mm around the annotated lesion as part of the masked region of interest (blue dashed line in Fig. 6) provided best AUC of 0.930 for fibroadenoma/carcinoma differentiation (Fig. 5). With this evaluation mask, the criterion ΔSoS of 43.16 m/s provided sensitivity of 80% and specificity of 100%. Restricting ΔSoS evaluation to the masked regions also eliminated the false-positive FA4, which occurs outside the lesion's actual position, and FA9, because a higher cutoff value could be applied. On the other hand, an additional false-negative CA3 was observed, because the observed ΔSoS increased did not match the masked region. Repeated measurements were available for 3 lesions (CA6, CA8, FA2). For each case, the lesion was relocated in B-mode and reassessed with SoS. The peak ΔSoS values in the repeated measurements (106.7 m/s for CA6, 78.8 m/s for CA8, and 17.8 m/s for FA2) were reproducible with respect to the first measurements in Tables 1 and 2, with (1 m/s, 0.4 m/s, and 10.5 m/s) ΔSoS uncertainties, respectively.

Of the 318 available SoS measurements in healthy women, 18/318 (6%) were excluded due to lack of acoustic coupling and 42/318 (13%) were excluded due to low-quality tissue displacement maps (only <60% of tissue displacement pixels available). From the remaining 258 segments, 61/258 (24%) were classified as ACR type A, 105/258 (41%) as type B, 62/258 (24%) as type C, and 30/258 (12%) as type D. We found a significant SoS difference between carcinoma lesions and each of the healthy tissue segment types ($P < 0.001$ for both ACR types A, B, C, and D; Fig. 7A). After ROC analysis, the criterion ΔSoS greater than 41.17 m/s provided sensitivity of 90%, specificity of 96.5%, and AUC of 0.938 (Fig. 7B). The ΔSoS comparison of fibroadenomas with each of the 4 differently dense healthy tissue was not significant. No significant ΔSoS difference was found when comparing the healthy tissues of different density categories among each other.

DISCUSSION

This study shows that breast cancer can be differentiated from fibroadenoma and healthy tissue of any density category using tissue reflections. The lesion localization in SoS-US images was consistent with B-mode imaging and repeated SoS-US measurements were reproducible. The technology works on standard US hardware, with a custom add-on software and a user interface developed for this purpose. The method can be applied to detect breasts with cancerous tumors and to differentiate between different lesion types.

SoS-US measurements have been performed in the past decade in several centers worldwide with special 3-dimensional (3D) US tomography machines. For a commercial 3D-USCT SoS measurement system, Duric et al[25] showed intermediate and high SoS, as well as attenuation for carcinoma (n = 38), while fibroadenoma (n = 31) exhibited lower values (specificity, 83.9%; sensitivity, 100%). The cutoff value was an SoS increase by 2.42%, which is equivalent to ΔSoS greater than 36 m/s, in good agreement with the cutoff values and

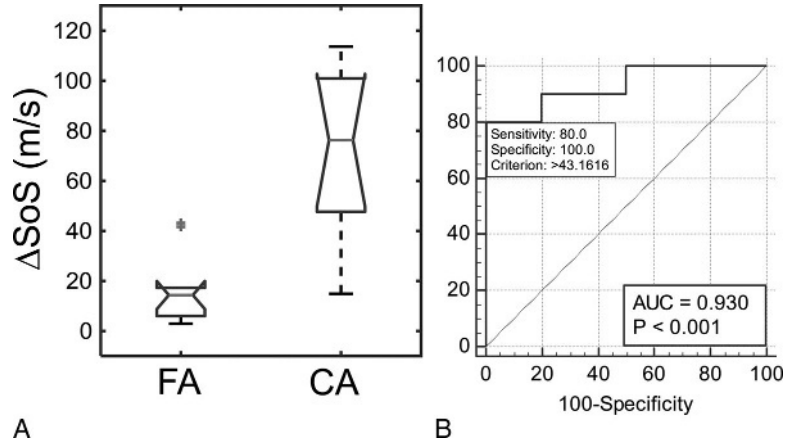

FIGURE 5. ANOVA (A) and ROC (B) plots for differentiation of fibroadenoma (FA) and carcinoma (CA). The evaluation is restricted to the lesion regions annotated in the B-mode by the sonographer augmented by a peritumorial region of 6 mm (blue dashed line in Fig. 6).

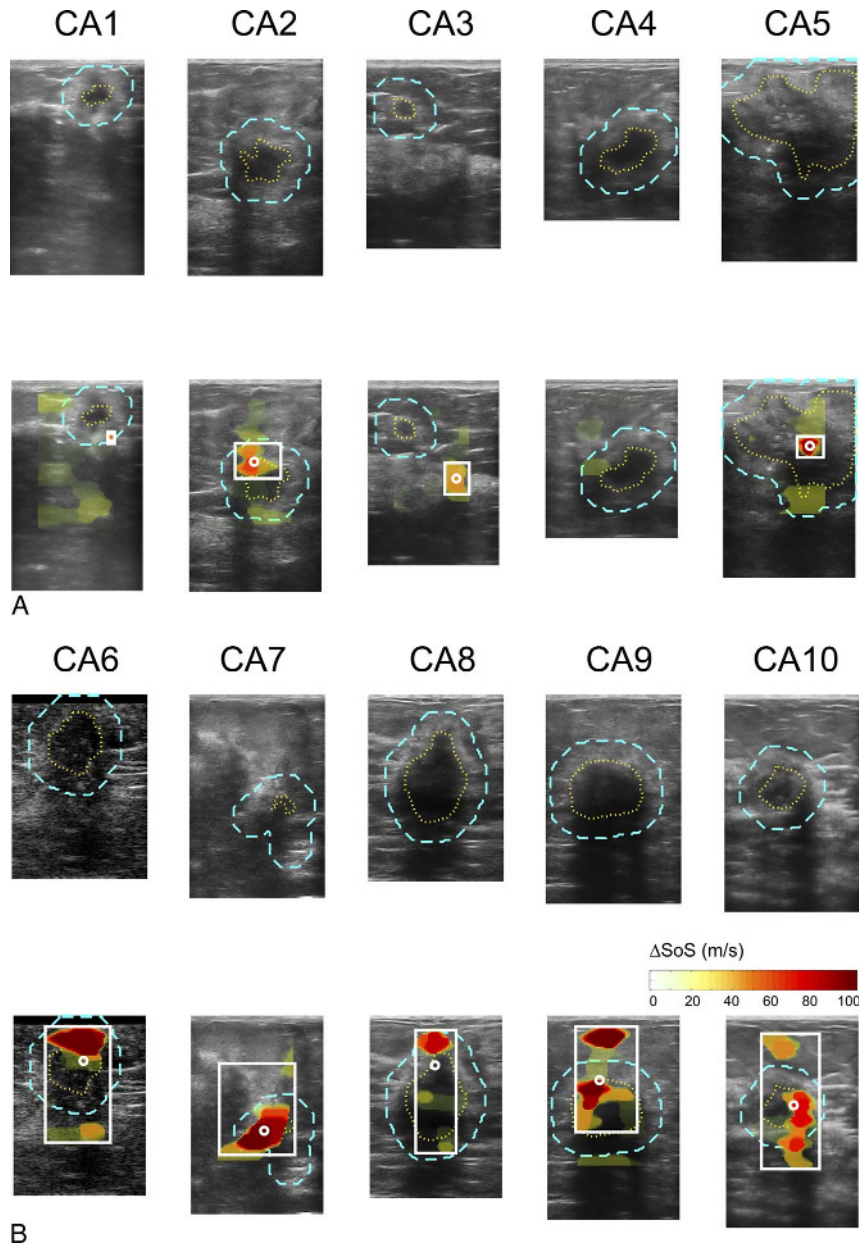

FIGURE 6. Carcinoma (CA) localization in SoS images (second and fourth rows) with respect to the lesion regions annotated in the B-mode by the sonographer (first and third rows). Sonographer annotations (yellow dotted line) were dilated with a radius of 6 mm to capture the peritumorial region (blue dashed line). The centroid position of the ΔSoS tumor images (white marker) and their bounding box with respect to a 50% threshold of the 42 m/s cutoff value (solid white line) are automatically extracted from the SoS images and shown as a reference. Seven of 10 lesions show a centroid within the B-mode lesion annotation region. CA1 has a centroid within the peritumorial region and CA3 outside the marked lesion region.

specificity observed in our pilot study. Using a method fusing USCT images and x-ray mammograms, Hopp et al[43] presented a technique promising for the differentiation of tumors and healthy tissue. Using a system combining transmission and reflection,[28] André et al were able to differentiate fibroadenoma (n = 11) from carcinoma (n = 5) with a specificity of 81.8% and sensitivity of 100%. Using a similar system, Iuanow et al[44] demonstrated differentiation of cysts from solid lesions. Three-dimensional multimodal US tomography combines multiple acoustic parameters into a composite index and has shown the capacity to distinguish malignant lesions from healthy tissue as well as from benign lesions and to detect small breast lesions.[26,27,29] From the available literature evidence, it cannot be concluded that ΔSoS in tumors is different for breast of different densities.[26,43,45–47] The SoS increase in tumors has been referred to microstructural distortion and densification of healthy tissues,[26,48] in which case a significant ΔSoS increase can be hypothesized regardless of the density of the breast. To the best of our knowledge, significant differences between ΔSoS in IDC and ILC have not been reported in the literature, and more sophisticated multiparametric biomarkers may be necessary to differentiate between different breast cancer subtypes.[26,43,48,49]

Compared with 3D-US tomography, our novel 2D technique has several advantages. The technique can be performed with standard US hardware in any body position. The method does not require a large, degassed, hygienic water bath, prone position, or dedicated table. The

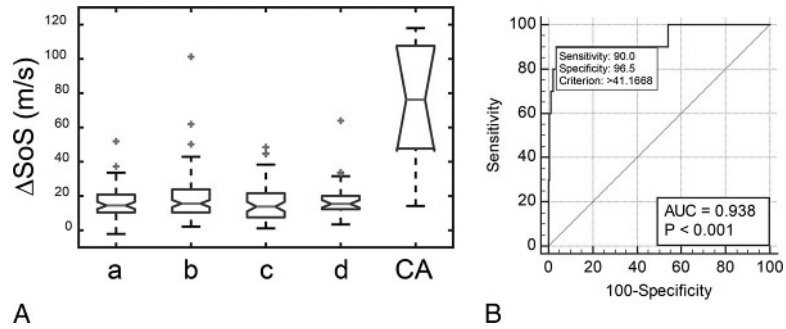

FIGURE 7. ANOVA (A) and ROC (B) plots for differentiation of carcinoma (CA) and healthy breast tissue for breast segments of different ACR mammographic density categories (A, B, C, D). The evaluation is based on the fully reconstructed SoS image.

corresponding equipment cost is low, and the necessary clinical space is small. The measurement time is reduced. This pilot study showed that SoS-US measurements were easily and rapidly performed and well tolerated. There was no need for a contrast agent or breast compression.

The method described by Sanabria et al.[34] and studied in this article for breast cancer could be used for differentiating solid breast lesions. Further studies are needed to assess the benefit in the differentiation between BI-RADS 3 and 4 lesions. This could potentially reduce the number of false-positive biopsies as well as the number of falsely down-staged lesions. Similarly to what has already been shown for US by Sannachi et al[50] and for SoS US by Lupinacci et al,[51] SoS-US could potentially be used as a fast and easy tool to predict the tumor response to chemotherapy. The current resolution is too low to make a conclusive statement on inner lesion structure. We are currently improving the signal-to-noise ratio of our prototype to increase the correlation in tissue displacement measures. A combination with diffraction tomography as reported by Huthwaite et al[52] and Simonetti et al[53] or full waveform inversion algorithms as presented by Wang et al[54] could present additional ways to improve the resolution and enable an improved insight into inner lesion characteristics.[55]

Our current installment contains some limitations, such as nonsimultaneous acquisitions of the B-mode image and SoS, which decreases the accuracy of the mask. We also observed bad coupling in the borderline areas, which was associated with high SoS values. The lack of whole breast coverage presents a further limitation. These limitations are of technical nature and can be improved with further refining of the data acquisition platform to achieve real-time visualization of SoS images in parallel to the B-mode, as it is nowadays possible with other elastography modalities.[10,11,22,56,57] There is potential for technological improvement in the lesion geometric delineation, for instance through improved image reconstruction and displacement tracking strategies, which would be necessary to analyze intratumor heterogeneity. Accordingly, in this current study, we considered the maximum ΔSoS values as a biomarker, which already shows the feasibility for cancer diagnosis. The proposed algorithm also depends on the availability of rich tissue texture to track phase displacements from different angular directions. Similarly to preceding 3D-USCT SoS studies, some overlap between SoS of fibroadenoma and carcinoma was found, which may be reduced with composite biomarkers (multiparametric imaging). Given the small sample size, most of the included breast cancers were incidentally in an elderly population. Although no significant difference in ΔSoS was found between cancerous lesions in dense (ACR type C) and nondense breasts (ACR types A and B), a larger study is necessary to cover patients in a wider age range and lesions in breasts of all density categories to validate the cutoff point of the ROC. The optimum ΔSoS cutoff point determined in this study should also be applied prospectively to an independent sample.

In conclusion, using SoS-US based on conventional US hardware and internal tissue reflections, breast carcinoma showed significant higher SoS values than fibroadenoma and healthy breast tissue of different densities.

ACKNOWLEDGMENT

The authors also thank Milka Cebic-Paunovic, Radiology Technologist for her valuable contributions.

REFERENCES

1. Torre LA, Islami F, Siegel RL, et al. Global cancer in women: burden and trends. *Cancer Epidemiol Biomarkers Prev.* 2017;26:444–457.
2. Guray M, Sahin AA. Benign breast diseases: classification, diagnosis, and management. *Oncologist.* 2006;11:435–449.
3. Kolb TM, Lichy J, Newhouse JH. Comparison of the performance of screening mammography, physical examination, and breast US and evaluation of factors that influence them: an analysis of 27,825 patient evaluations. *Radiology.* 2002;225:165–175.
4. Buchberger W, Niehoff A, Obrist P, et al. Clinically and mammographically occult breast lesions: detection and classification with high-resolution sonography. *Semin Ultrasound CT MR.* 2000;21:325–336.
5. Gordon PB, Goldenberg SL. Malignant breast masses detected only by ultrasound. A retrospective review. *Cancer.* 1995;76:626–630.
6. Yoon GY, Cha JH, Kim HH, et al. Sonographic features that can be used to differentiate between small triple-negative breast cancer and fibroadenoma. *Ultrasonography.* 2018;37:149–156.
7. Yeo SH, Kim GR, Lee SH, et al. Comparison of ultrasound elastography and color Doppler ultrasonography for distinguishing small triple-negative breast cancer from fibroadenoma. *J Ultrasound Med.* 2018;37:2135–2146.
8. Lee SH, Moon WK, Cho N, et al. Shear-wave elastographic features of breast cancers: comparison with mechanical elasticity and histopathologic characteristics. *Invest Radiol.* 2014;49:147–155.
9. Arribas EM, Whitman GJ, De Bruhl N. Screening breast ultrasound: where are we today? *Current Breast Cancer Reports.* 2016;8:221–229.
10. Barr RG, Nakashima K, Amy D, et al. WFUMB guidelines and recommendations for clinical use of ultrasound elastography: part 2: breast. *Ultrasound Med Biol.* 2015;41:1148–1160.
11. Berg WA, Cosgrove DO, Dore CJ, et al. Shear-wave elastography improves the specificity of breast US: the BE1 multinational study of 939 masses. *Radiology.* 2012;262:435–449.
12. Sadigh G, Carlos RC, Neal CH, et al. Accuracy of quantitative ultrasound elastography for differentiation of malignant and benign breast abnormalities: a meta-analysis. *Breast Cancer Res Treat.* 2012;134:923–931.
13. Barr RG, Zhang Z. Effects of precompression on elasticity imaging of the breast: development of a clinically useful semiquantitative method of precompression assessment. *J Ultrasound Med.* 2012;31:895–902.
14. Vinnicombe SJ, Whelehan P, Thomson K, et al. What are the characteristics of breast cancers misclassified as benign by quantitative ultrasound shear wave elastography? *Eur Radiol.* 2014;24:921–926.
15. Kuhl CK. The changing world of breast cancer: a radiologist's perspective. *Invest Radiol.* 2015;50:615–628.
16. Pinker K, Moy L, Sutton EJ, et al. Diffusion-weighted imaging with apparent diffusion coefficient mapping for breast cancer detection as a stand-alone parameter: comparison with dynamic contrast-enhanced and multiparametric magnetic resonance imaging. *Invest Radiol.* 2018;53:587–595.

17. Erhard K, Kilburn-Toppin F, Willsher P, et al. Characterization of cystic lesions by spectral mammography: results of a clinical pilot study. *Invest Radiol*. 2016;51: 340–347.
18. Hauser N, Wang Z, Kubik-Huch RA, et al. A study on mastectomy samples to evaluate breast imaging quality and potential clinical relevance of differential phase contrast mammography. *Invest Radiol*. 2014;49:131–137.
19. Sayed A, Layne G, Abraham J, et al. Nonlinear characterization of breast cancer using multi-compression 3D ultrasound elastography in vivo. *Ultrasonics*. 2013; 53:979–991.
20. Goenezen S, Dord JF, Sink Z, et al. Linear and nonlinear elastic modulus imaging: an application to breast cancer diagnosis. *IEEE Trans Med Imaging*. 2012;31: 1628–1637.
21. Lassau N, Coiffier B, Faivre L, et al. Study of intrapatient variability and reproducibility of quantitative tumor perfusion parameters evaluated with dynamic contrast-enhanced ultrasonography. *Invest Radiol*. 2017;52:148–154.
22. Neuschler EI, Butler R, Young CA, et al. A pivotal study of optoacoustic imaging to diagnose benign and malignant breast masses: a new evaluation tool for radiologists. *Radiology*. 2018;287:398–412.
23. Butler R, Lavin PT, Tucker FL, et al. Optoacoustic breast imaging: imaging-pathology correlation of optoacoustic features in benign and malignant breast masses. *AJR Am J Roentgenol*. 2018;211:1155–1170.
24. Becker AS, Marcon M, Ghafoor S, et al. Deep learning in mammography: diagnostic accuracy of a multipurpose image analysis software in the detection of breast cancer. *Invest Radiol*. 2017;52:434–440.
25. Duric N, Littrup P, Chandjwala-Mody P, et al. In-vivo imaging results with ultrasound tomography: report on an ongoing study at the Karmanos Cancer Institute. *Proc SPIE 7629, Medical Imaging 2010: Ultrasonic Imaging, Tomography, and Therapy*. 2010;76290M.
26. Zografos G, Liakou P, Koulocheri D, et al. Differentiation of BIRADS-4 small breast lesions via multimodal ultrasound tomography. *Eur Radiol*. 2015;25:410–418.
27. Zografos G, Koulocheri D, Liakou P, et al. Novel technology of multimodal ultrasound tomography detects breast lesions. *Eur Radiol*. 2013;23:673–683.
28. Andre MP, Barker CH, Sekhon N, et al. Pre-clinical experience with full-wave inverse-scattering for breast imaging. In: Akiyama I, ed. *Acoustical Imaging* vol. 29. Dordretch, Holand: Springer; 2008.
29. Forte S, Dellas S, Stieltjes B, et al. Multimodal ultrasound tomography for breast imaging: a prospective study of clinical feasibility. *Eur Radiol Exp*. 2017;1:27.
30. Benjamin A, Zubajlo R, Dhyani M, et al. Non-invasive diagnosis of non-alcoholic fatty liver disease (NAFLD) using Ultrasound Image Echogenicity. *Conf Proc IEEE Eng Med Biol Soc*. 2017;2017:2920–2923.
31. Cho S, Kang J, Lee Y, et al. Phantom and in-vivo evaluation of sound speed estimation methods: preliminary results. *IEEE Intern Ultrasonics Symposium*. 2014; 1678–1681.
32. Imbault M, Faccinetto A, Osmanski BF, et al. Robust sound speed estimation for ultrasound-based hepatic steatosis assessment. *Phys Med Biol*. 2017;62:3582–3598.
33. Jaeger M, Frenz M. Towards clinical computed ultrasound tomography in echo-mode: dynamic range artefact reduction. *Ultrasonics*. 2015;62:299–304.
34. Sanabria SJ, Ozkan E, Rominger M, et al. Spatial domain reconstruction for imaging speed-of-sound with pulse-echo ultrasound: simulation and in-vivo study. *Phys Med Biol*. 2018;63:215015.
35. Sanabria SJ, Goksel O, Martini K, et al. Breast-density assessment with hand-held ultrasound: a novel biomarker to assess breast cancer risk and to tailor screening? *Eur Radiol*. 2018;28:3165–3175.
36. Sanabria SJ, Martini K, Freystatter G, et al. Speed of sound ultrasound: a pilot study on a novel technique to identify sarcopenia in seniors. *Eur Radiol*. 2019;29:3–12.
37. American College of Radiology. *ACR BI-RADS Atlas: Breast Imaging Reporting and Data System (5th ed)*. Reston, VA: American College of Radiology; 2013.
38. Hoskins P, Martin K, Thrush A. *Diagnostic Ultrasound Physics and Equipment, 2nd ed*. Cambridge, United Kingdom: Cambridge Medicine; 2010.
39. Shung KK, Thieme GA. *Ultrasound scattering in biological tissues*. Boca Raton, FL: CRC Press; 1993.
40. Stavros AT. *Breast ultrasound*. Philadelphia, PA: Lippincott Williams & Wilkins; 2004.
41. Vreemann S, Rodriguez-Ruiz A, Nickel D, et al. Compressed sensing for breast MRI: resolving the trade-off between spatial and temporal resolution. *Invest Radiol*. 2017;52:574–582.
42. Zweig MH, Campbell G. Receiver-operating characteristic (ROC) plots: a fundamental evaluation tool in clinical medicine. *Clin Chem*. 1993;39:561–577.
43. Hopp T, Duric N, Ruiter NV. Image fusion of ultrasound computer tomography volumes with x-ray mammograms using a biomechanical model based 2D/3D registration. *Comput Med Imaging Graph*. 2015;40:170–181.
44. Iuanow E, Smith K, Obuchowski NA, et al. Accuracy of cyst versus solid diagnosis in the breast using quantitative transmission (QT) ultrasound. *Acad Radiol*. 2017;24:1148–1153.
45. André M, Barker C, Sekhon N, et al. Pre-clinical experience with full-wave inverse-scattering for breast imaging. *Acoustical Imaging*. 2008;29.
46. Duric N, Littrup P, Chandiwala-Mody P, et al. In-vivo imaging results with ultrasound tomography: report on an ongoing study at the Karmanos Cancer Institute. *Proc. SPIE 7629, Medical Imaging 2010: Ultrasonic Imaging, Tomography, and Therapy*. 2010.
47. Zografos GN, Koulocheri D, Liakou P, et al. Detection of breast cancer via 3D multi-modal ultrasound tomography. *ECR*. 2011;C-1135:2011.
48. Greenleaf JF, Bahn RC. Clinical imaging with transmissive ultrasonic computerized tomography. *IEEE Trans Biomed Eng*. 1981;28:177–185.
49. Liovarou I, Zografos GM, Koulocheri D, et al. Clinical use of multimodal ultrasound tomography (MUT) for breast cancer detection. *ECR 2014*; Poster No.: C-0845. 2014.
50. Sannachi L, Gangeh M, Tadayyon H, et al. Response monitoring of breast cancer patients receiving neoadjuvant chemotherapy using quantitative ultrasound, texture, and molecular features. *PLoS One*. 2018;13:e0189634.
51. Lupinacci J, Duric N, Littrup P, et al. Monitoring breast masses with ultrasound tomography in patients undergoing neoadjuvant chemotherapy. *Medical Imaging 2010: Ultrasonic Imaging, Tomography, and Therapy*. 2010;7629.
52. Huthwaite P, Simonetti F, Duric N. Combining time of flight and diffraction tomography for high resolution breast imaging: initial in vivo results (L). *J Acoust Soc Am*. 2012;132:1249–1252.
53. Simonetti F, Huang L, Duric N, et al. Diffraction and coherence in breast ultrasound tomography: a study with a toroidal array. *Med Phys*. 2009;36:2955–2965.
54. Wang K, Matthews T, Anis F, et al. Waveform inversion with source encoding for breast sound speed reconstruction in ultrasound computed tomography. *IEEE Trans Ultrason Ferroelectr Freq Control*. 2015;62:475–493.
55. Duric N, Littrup P, West E, et al. In-vivo imaging of breast cancer with ultrasound tomography: probing the tumor environment. *SPIE Medical Imaging*. 2011; SPIE: 7.
56. Zhang Q, Suo J, Chang W, et al. Dual-modal computer-assisted evaluation of axillary lymph node metastasis in breast cancer patients on both real-time elastography and B-mode ultrasound. *Eur J Radiol*. 2017;95:66–74.
57. Sigrist RMS, Liau J, Kaffas AE, et al. Ultrasound elastography: review of techniques and clinical applications. *Theranostics*. 2017;7:1303–1329.